Matter and Radiation at Extremes | RESEARCH ARTICLE | scitation.org/journal/mre

Effect of ablation on the nonlinear spike growth for the single-mode ablative Rayleigh–Taylor instability

Cite as: Matter Radiat. Extremes 8, 016901 (2023); doi: 10.1063/5.0106832
Submitted: 30 June 2022 • Accepted: 30 November 2022 •
Published Online: 5 January 2023

J. Y. Fu,[1] H. S. Zhang,[2,a)] H. B. Cai,[2] P. L. Yao,[3] and S. P. Zhu[2,3,4]

AFFILIATIONS

[1] Institute of Applied Physics and Computational Mathematics, Beijing 100088, People's Republic of China
[2] Laboratory of Computational Physics, Institute of Applied Physics and Computational Mathematics, Beijing 100088, People's Republic of China
[3] Graduate School, China Academy of Engineering Physics, P.O. Box 2101, Beijing 100088, People's Republic of China
[4] Science and Technology on Plasma Physics Laboratory, Laser Fusion Research Center, CAEP, Mianyang 621900, People's Republic of China

[a)] **Author to whom correspondence should be addressed:** zhang_huasen@hotmail.com

ABSTRACT

The effect of ablation on the nonlinear spike growth of single-mode ablative Rayleigh–Taylor instability (RTI) is studied by two-dimensional numerical simulations. It is shown that the ablation can reduce the quasi-constant velocity and significantly suppress the reacceleration of the spike in the nonlinear phase. It is also shown that the spike growth can affect the ablation-generated vorticity inside the bubble, which further affects the nonlinear bubble acceleration. The vorticity evolution is found to be correlated with the mixing width (i.e., the sum of the bubble and spike growths) for a given wave number and ablation velocity. By considering the effects of mass ablation and vorticity, an analytical model for the nonlinear bubble and spike growth of single-mode ablative RTI is developed in this study. It is found that the nonlinear growth of the mixing width, induced by the single mode, is dominated by the bubble growth for small-scale ablative RTI, whereas it is dominated by the spike growth for classical RTI.

I. INTRODUCTION

Rayleigh–Taylor instability (RTI)[1,2] is a commonly occurring phenomenon in many natural and engineering systems. Classical RTI (CRTI) usually arises when a lighter fluid is pushed toward a heavier fluid by an external force, and spikes (bubbles) form when the heavy (light) fluid, of density ρ_h (ρ_l) penetrates into the light (heavy) fluid. RTI can cause mixing, which is determined by the penetration depths (i.e., the mixing widths) of the bubble h_b and the spike h_s. This mixing process plays an important role in, for example, inertial confinement fusion (ICF)[3] and supernova (SN) explosions.[4] In ICF, a cold dense shell is accelerated by the pressure caused by the ablation of the shell into a hot, low-density plasma, and the RTI is then affected by the mass ablation at the interface. The RTI in this case is often termed ablative RTI (ARTI), as opposed to CRTI. In ICF implosions, ARTI-induced mixing can lead to degradation of implosion performance and to ignition failure.[5] ARTI also plays a significant role in SN explosions, where it can accelerate the deflagration front.[6]

According to linear CRTI theory,[1] a small perturbation will grow exponentially with time at a rate $\gamma_L^{cls} = \sqrt{A_T g k}$, where $A_T = (\rho_h - \rho_l)/(\rho_h + \rho_l)$ is the Atwood number, g is the gravitational or inertial acceleration, and k is the wave number. Compared with CRTI, the linear growth of ARTI is significantly reduced owing to mass ablation.[7–12] The ARTI linear growth rate can be written as[12]

$$\gamma_L^{abl} = \sqrt{A_T g k - \frac{A_T^2 k^2 V_a^2}{r_d}} - (1 + A_T) k V_a$$

for large Froude numbers $F_r = V_a^2/g\,L_0$, where $V_a = \dot{m}_a/\rho_h$ is the ablation velocity, $\dot{m}_a$ is the ablation rate, $r_d = \rho_l/\rho_h$ is the fluid density ratio, and L_0 is the thickness of the ablation front. Mass ablation leads to a linear cutoff wave number k_c beyond which the ARTI modes are linearly stable ($\gamma_L^{abl} \le 0$). Nevertheless, it has been demonstrated that linearly stable ARTI modes can be destabilized by a finite-amplitude initial perturbation.[13,14]

It has been found that the single-mode CRTI bubble front can reach a quasi-constant velocity

$$V_b^{cls} = \sqrt{\frac{2A_T}{1+A_T}\frac{g}{C_g k}}$$

in the nonlinear phase,[15–17] and this has been verified by simulations[18–21] and experiments.[22] Here, C_g is a constant having a value 3 or 1 for a two-dimensional (2D) or three-dimensional (3D) geometry, respectively. During the nonlinear growth of single-mode ARTI,[13,14,23,24] the vorticity generated at the spike tip is convected toward the bubble vertex. Consequently, the bubble growth is accelerated by the vorticity-induced centrifugal force F_c, with a nonlinear bubble velocity

$$V_b^{abl} \approx \sqrt{\frac{2A_T}{1+A_T}\frac{g}{C_g k} + \frac{r_d\omega_0^2}{4k^2}}$$

greater than the classical value V_b^{cls}. Here, ω_0 is the strength of the vorticity $\nabla \times \boldsymbol{v}$, and $\boldsymbol{v}$ is the fluid velocity.

As concluded by Wei and Livescu,[25] the single-mode CRTI spike growth at large Reynolds numbers [defined by Eq. (3.2) in Ref. 25] exhibits three nonlinear growth regimes: a potential flow regime, a reacceleration regime, and a chaotic regime. In the potential flow regime, the spike growth can be described by potential flow theory,[15,16] with a quasi-constant velocity

$$V_s^{cls} = -\sqrt{\frac{2A_T}{1-A_T}\frac{g}{C_g k}}.$$

However, it has been found[21,22] that when A_T is close to unity, the spike growth goes through the reacceleration regime (i.e., keeps on accelerating) with an asymptotic acceleration a_s ($h_s \sim -0.5a_s t^2$, $a_s \le g$). This reacceleration is due to a reduction in frictional drag as a result of the formation of a vortex near the spike tip.[22,25,26] When A_T is equal to one, there is no frictional drag, and the spike follows exactly a free-fall behavior[27] $h_s \sim -0.5gt^2$. In the chaotic regime, the instability experiences random acceleration and deceleration phases as a result of complex vortical motions.[25]

For spike growth in single-mode ARTI, the formation of jet-like spike structures has been observed experimentally during the nonlinear growth of ARTI,[28,29] and Wang *et al.*[30] found that the preheating effect plays an essential role in this phenomenon. Furthermore, using a Layzer-type approach, Sanz *et al.*[31] discovered that nonlinear spike growth in single-mode ARTI can reach a reacceleration regime. Ye *et al.*[32] discovered that after the reacceleration regime, nonlinear spike growth during the evolution of single-mode ARTI can reach a deceleration regime. Although the stabilizing effect of ablation on ARTI in the linear regime has been extensively studied,[7–12] its effect on spike growth in the nonlinear regime is still not well understood.

In this work, we study the effect of ablation on nonlinear spike growth in single-mode ARTI. The results of simulations show that the ablative effect can reduce the quasi-constant velocity and significantly suppress the reacceleration of the spike in the nonlinear phase by ablating the spike and convecting vorticity from the spike to the bubble vertex. In addition, it is also found that the ARTI spike growth can affect the ablation-generated vorticity, which in turn can affect the bubble acceleration in the nonlinear regime. This vorticity is found to be correlated with the mixing width (i.e., the sum of the bubble and spike growths) for a given wave number k and ablation velocity V_a. The initial perturbation amplitude can affect the vorticity strength (at the same h_b) by affecting the contribution of h_b to the mixing width. Finally, an analytical model is developed for the nonlinear bubble and spike growth in single-mode ARTI by considering ablative and vorticity effects in a CRTI model.[33,34] The predictions of the ARTI model are in good agreement with data from numerical simulations. It is found that the nonlinear growth of the mixing width, induced by the single mode, is dominated by bubble growth in the case of small-scale (large-k) ARTI, whereas it is dominated by spike growth in the case of CRTI.

The remainder of this paper is organized as follows. Simulations of nonlinear ARTI spike growth are presented in Sec. II. The effects of the ARTI spike growth on the ablation-generated vorticity are discussed in Sec. III. Analytical modeling of the nonlinear growth of single-mode ARTI is described in Sec. IV. The conclusions drawn from this work are presented in Sec. V.

II. ABLATIVE EFFECT ON NONLINEAR SPIKE GROWTH

This section presents the details of the single-mode RTI simulations performed to study the effect of ablation on nonlinear spike growth. Here, we focus on the early-time dynamics (i.e., the potential flow regime and the reacceleration regime). The hydrodynamic code ART[23] is used, which solves the single-fluid equation with Spitzer–Härm thermal conduction[35] and an ideal gas equation of state. The details of ART can be found in Refs. 23, 24, and 36.

In conventional CRTI, uniform densities ρ_h and ρ_l of the heavy and light fluids, respectively, are usually used, whereas the density profile is smoothly varying in ARTI owing to thermal conduction, as shown in Fig. 1(a). The ARTI density profile is obviously different from that of conventional CRTI. Hence, in addition to the conventional CRTI and ARTI simulations, we also perform CRTI simulations with the ARTI density profile. In the simulations involving a smoothly varying density profile, the Atwood number is calculated using $A_T = (\rho_h - \rho_l)/(\rho_h + \rho_l)$, where ρ_h is the maximum density at the spike tip, and ρ_l is the density at a distance $2/k$ below the tip, as indicated by linear theory.[11] Since the initial A_T of ARTI depends on k [Fig. 1(b)], we can use k to represent A_T in the ARTI studies. It should be noted that A_T is independent of k in conventional CRTI because of the short density gradient scale length ($L_m \ll k^{-1}$) at the fluid interface.

The simulations are carried out within a computational box of 110 μm in the Z direction and with wavelength $\lambda = 2\pi/k$ of the single-mode perturbation in the X direction. On the basis of convergence studies, the grid numbers are taken as 2200 and 220 in the Z and X directions, respectively. At the initial time of the simulations, the RTI is seeded by a velocity perturbation in both directions near the fluid interface $Z = Z_0$. The perturbation has

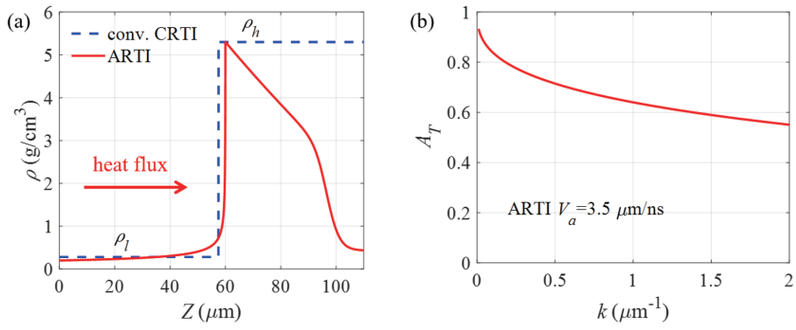

FIG. 1. (a) Initial equilibrium density profiles in the simulations of conventional CRTI and ARTI. (b) Dependence of the initial Atwood number A_T on wave number k in the ARTI simulations.

the form $V_{pz} = V_{p0}\cos(kX)\exp(-k|Z - Z_0|)$ in the Z direction and $V_{px} = V_{p0}\sin(kX)\exp(-k|Z - Z_0|)$ in the X direction, which is the same as the perturbation used by Zhang *et al.*[14] In the ARTI simulations, the bubble/spike penetration velocities $V_{b/s}$ are computed as the velocity of the bubble and the spike vertex relative to the velocity of the dense target averaged in the X direction. The penetration depths of the bubble and the spike, $h_{b/s}$, are obtained by integrating $V_{b/s}$ over time.

A periodic boundary condition is used at the left ($X = 0$) and right ($X = \lambda$) boundaries in all the simulations. In the CRTI simulations, all the parameters at the bottom ($Z = 0$) and top ($Z = 110\ \mu$m) boundaries remain equal to their initial values. In the ARTI simulations, a constant heat flux (5.0 MW/μm^2) is applied at the bottom boundary to simulate the energy flux toward the ablation front from the laser-absorption region, as shown in Fig. 1(a). The value of the heat flux is determined from the initial equilibrium. The top boundary is set to be adiabatic, and $\partial_Z V_z = 0$ is used for the inflow boundary condition,[36] where V_z is the velocity component in the Z direction.

First, we perform conventional CRTI simulations with $k = 0.78\ \mu$m^{-1}. The simulated histories of the spike velocities V_s are shown in Fig. 2(a). Here, we focus on $A_T \geq 0.5$, because that is the usual parameter range of ARTI [Fig. 1(b)]. At early times ($t \lesssim 0.6$ ns), V_s grows exponentially in the linear regime. Then, in the potential flow regime, V_s approaches a nearly constant value (at about $t = 1.0$ ns), which is slightly greater than the theoretical quasi-constant velocity[15,16,25] V_s^{cls}. The nearly constant value of V_s is defined here as the simulated quasi-constant spike velocity V_s^{qc}, which can be identified by a local minimum slope in the velocity history. Finally, as a result of the formation of spike vortices,[26] the spike growth transitions into the reacceleration regime with an asymptotic acceleration a_s. It is found that a_s increases with increasing A_T, which is consistent with the CRTI simulations presented in previous studies.[19–21,25,26] It is further found that the normalized spike acceleration $a_s/2gA_T$ has a value of ~0.3 that is not sensitive to A_T when $A_T = 0.5$–0.9 [Fig. 2(b)]. This is different from the results of a previous 3D CRTI study,[21] where $a_s/2gA_T$ had a value of ~0.3 when $A_T = 0.9$, and decreased with decreasing A_T when $A_T = 0.6$–0.9. The discrepancy is possibly due to the dimensional difference between Ref. 21 and this work.

Next, we study the effect of ablation on single-mode ARTI spike growth, in which the simulation parameters are taken to be similar to those in our previous work.[14,37,38] The ablation velocity $V_a = 3.5\ \mu$m/ns, and the initial acceleration $g_0 = 100\ \mu$m/ns^2, corresponding to the acceleration phase in a typical direct-drive target designed for the National Ignition Facility (NIF).[39] As shown in Fig. 1(a), the initial ablation front is located at $Z_0 = 60\ \mu$m, and the maximum density is $\rho_a = 5.3$ g/cm^2. At the ablation front, the minimum density gradient scale length is $L_m \approx 0.162\ \mu$m, and the pressure is $P_a = 220$ Mbar. Based on these parameters and linear theory,[11,12] the thickness of the ablation front $L_0 \approx 0.124L_m \approx 0.02\ \mu$m, the cutoff wave number $k_c = 1.19\ \mu$m^{-1}, and the Froude number $F_r = 6.13$.

Figure 3(a) shows the evolution of the spike velocity V_s in the single-mode CRTI simulations with the ARTI density profile. Similar to the results of the conventional CRTI simulations shown in

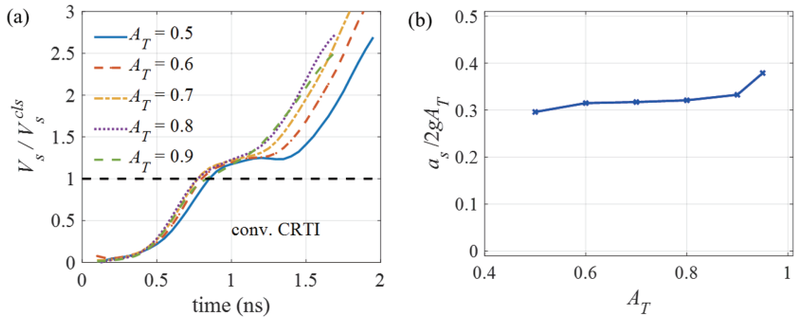

FIG. 2. (a) Histories of the spike velocities V_s in the conventional single-mode CRTI simulations. (b) Dependence of the spike accelerations a_s on A_T in the reacceleration regime.

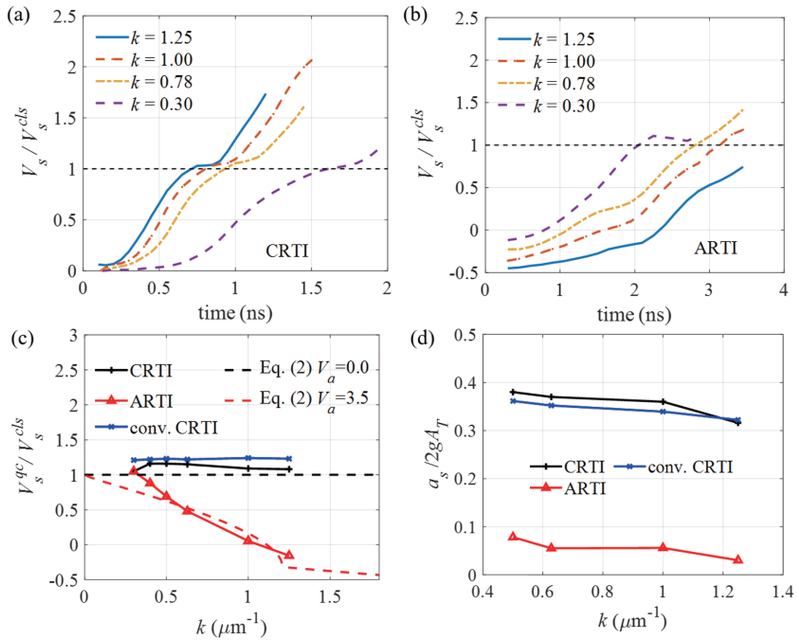

FIG. 3. History of the spike velocity V_s from (a) the CRTI simulations with the ARTI density profile and (b) the ARTI simulations. (c) and (d) Dependences of V_s^{qc} on k and of a_s on k in the CRTI simulations with the ARTI density profile, the conventional CRTI simulations, and the ARTI simulations. The dashed lines in (c) are the solutions of Eq. (2) for each case.

Fig. 2, the evolution of the spikes in the CRTI simulations with the ARTI density profile can also be divided into a linear regime, a potential flow regime (with quasi-constant velocity V_s^{qc}), and a reacceleration regime (with asymptotic acceleration a_s). For comparison, we also carry out conventional CRTI simulations using the same A_T as the CRTI modes in the ARTI density profile. The values of V_s^{qc} and a_s from these CRTI simulations are plotted in Figs. 3(c) and 3(d). It can be seen that V_s^{qc} and a_s obtained from the CRTI simulations with the ARTI density profile are very close to those obtained from the conventional CRTI simulations. This indicates that the ARTI density profile has little effect on the nonlinear spike growth in comparison with the density profile of the conventional CRTI.

Figure 3(b) shows the evolution of the simulated V_s of the different ARTI modes. In the linear regime,[7–12] it is found that the ARTI linear growth rate γ_L^{abl} decreases as k increases when $k > k_{max} \approx 0.3\ \mu m^{-1}$, where k_{max} is the wave number at which $\gamma_L^{abl}(k)$ has its greatest value. In the potential flow regime, V_s of ARTI can reach a quasi-constant value V_s^{qc}, although the local minimum slope of the V_s history in the ARTI cases is less obvious than that in the CRTI cases. Also, the values of V_s^{qc} in the ARTI cases for large k are smaller than those in the CRTI cases, indicating that ablation alters the global behavior of V_s evolution. The ARTI spike growth also goes through a reacceleration regime, in which the asymptotic spike acceleration a_s is much smaller than that of CRTI. It is further found that both V_s^{qc} and a_s in the ARTI simulations are insensitive to the initial perturbation amplitude V_p in the investigated parameter range $0 < V_p < V_a$ (data not shown in figure).

Figure 3(c) shows the dependence of the simulated V_s^{qc} on k. For small values of k, V_s^{qc} is close to the classical value, whereas as k increases, V_s^{qc} decreases, a trend consistent with the enhancement of the ablative effect. The mode for $k = 1.25\ \mu m^{-1} > k_c$ is destabilized by a finite-amplitude initial perturbation,[13,14] and the negative spike growth of the mode ($V_s^{qc}/V_s^{cls} < 0$) indicates that the spike growth is strongly suppressed by mass ablation. We further use the drag-buoyancy model[17] to analyze the relation between V_s^{qc} and k. The steady-state drag-buoyancy model for the single-mode CRTI spike has the form

$$(\rho_h - \rho_l)g = C_d\, k\, \rho_l V_s^2, \tag{1}$$

where $C_d = 3$ is the drag coefficient for 2D CRTI. In a unit volume of the spike element, the buoyancy force on the left-hand side cancels out the drag force on the right-hand side. As a result, $V_s = V_s^{cls}$. In ARTI, the ablative effect[31] can generate a perturbed dynamic pressure $\delta P_a \sim \rho_h V_a^2$, and a restoring force $F_a = -\partial \delta P_a/\partial Z \sim C_a k \rho_h V_a^2$ at the spike tip, where C_a is the ablative restoring coefficient to be determined later. Thus, Eq. (1) can be rewritten as

$$(\rho_h - \rho_l)g - C_a k \rho_h V_a^2 = C_d k \rho_l (V_s - V_a)^2, \tag{2}$$

where $V_s - V_a$ is the spike velocity relative to the ambient fluid. When the ARTI is linearly unstable ($k < k_c$), the solution for the spike velocity is

$$V_s = V_s^{cls}\sqrt{1 - \frac{C_a k V_a^2}{(1 - r_d)g}} + V_a.$$

When the ARTI is linearly stable ($k \geq k_c$), the spike velocity should be $V_s = V_a$, owing to the ablation-induced interface motion. An ablative restoring coefficient $C_a = g(1 - r_d)/V_a^2 k_c \approx 7$ is obtained at $k = k_c$. It is found that the solution of Eq. (2) agrees qualitatively with the dependence of V_s^{qc} on k and V_a in Fig. 3(c).

Finally, to investigate the effect of ablation on the spike growth in the reacceleration regime, we compare the asymptotic spike accelerations a_s in the CRTI and ARTI simulations, as shown in Fig. 3(d). Compared with CRTI, the a_s corresponding to ARTI is significantly suppressed. Furthermore, as k increases, the ablative effect increases, resulting in a smaller a_s at a larger k. Unlike the quasi-constant spike velocity V_s^{qc} [Fig. 3(c)], the difference between the a_s of ARTI and CRTI does not decrease as k decreases, indicating that the ablative effect on a_s is less sensitive to k compared with the ablative effect on V_s^{qc} in the investigated k range.

We further compare the vorticity ω_0 structure and the mode structure in the spike reacceleration regime of the CRTI and ARTI, as shown in Fig. 4. For CRTI [Fig. 4(a)], the vorticity is strong near the spike tip, which is closely related to the spike reacceleration.[22,25,26] For ARTI [Fig. 4(b)], the vorticity near the spike is much weaker than that in CRTI, which can result in a lower value of a_s in ARTI than in CRTI [Fig. 3(d)]. The vorticity in ARTI is convected from the spike to the bubble by the ablation flow, thus leading to a weak vorticity ω_0 near the spike.[23] Furthermore, during the evolution of single-mode CRTI, a spike with a higher velocity V_s tends to have higher velocity shear $\partial_X V_Z$ and vorticity ω_0 in the vicinity.[40] Because of mass ablation, V_s in the reacceleration regime of ARTI is reduced compared with that of CRTI (Fig. 3), and this can contribute to a weak velocity shear $\partial_X V_Z$ and a weak vorticity ω_0 near the ARTI spike. On the other hand, the CRTI spike has a characteristic mushroom structure induced by Kelvin–Helmholtz instability (KHI), the linear growth rate of which increases with increasing velocity shear.[41] In ARTI, the mushroom structure is not visible, indicating that KHI is stabilized. This phenomenon is consistent with the results of ARTI simulations from previous studies[30,32] and is possibly due to the ablation stabilization effect,[42] as well as to the ablation-induced reduction of velocity shear (i.e., the driving term).

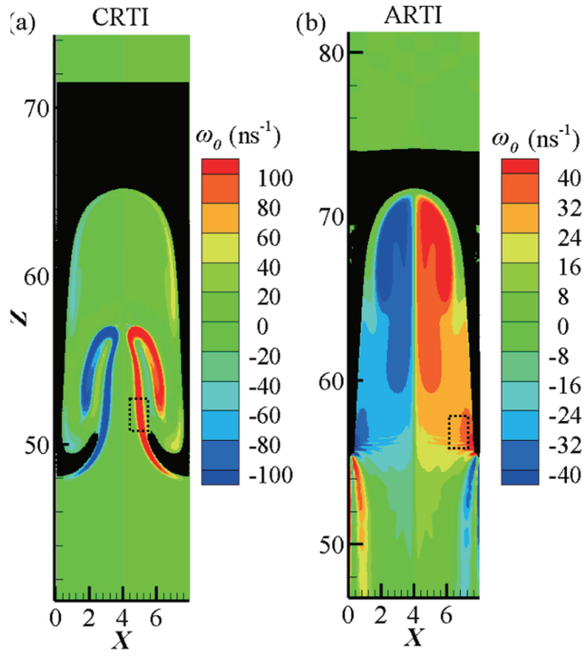

FIG. 4. 2D vorticity ω_0 structures in the spike reacceleration regime from the single-mode CRTI simulation (with ARTI density profile) and the ARTI simulation for $k = 0.78\ \mu m^{-1}$: (a) CRTI at $t = 1.30$ ns; (b) ARTI at $t = 2.25$ ns. The black regions are the high-density fluid. The black rectangular boxes indicated the areas where the volume average of the velocity shear $\partial_X V_Z$ is measured. The volume average of $\partial_X V_Z$ has values of ~106.0 and ~23.0 ns^{-1} in (a) and (b), respectively.

III. EFFECT OF SPIKE GROWTH ON THE EVOLUTION OF VORTICITY IN ARTI

In this section, we study the effect of ARTI spike growth on the evolution of vorticity. First, we investigate the relationship between the vorticity strength ω_0 and the ARTI mixing width $W_{b-s} = h_b - h_s$. The vorticity strength ω_0 at the bubble vertex is calculated by performing a volume integration of $|\nabla \times \boldsymbol{v}|$ between the bubble vertex and a distance ~$1/k$ from the vertex into the bubble, identical to previous studies of ARTI.[14,23] Here, $|\cdots|$ indicates the magnitude of a vector.

Figure 5 shows the evolution of ω_0 at the bubble vertex in single-mode ARTI simulations. For the same wave number k [e.g., in Fig. 5(b)], the evolution of the normalized vorticity strength $\hat{\omega} = \omega_0 r_d / k V_a$ is related only to the normalized mixing width $\hat{W} = W_{b-s}/\lambda$, and is not sensitive to the initial perturbation amplitude V_p. With the growth of $\hat{W}$, $\hat{\omega}$ approaches an asymptotic value. It is found that this relation can be roughly fitted by $\hat{\omega} = 2.8\hat{W}^{1.5}/(1.8 + \hat{W}^{1.5})$, indicating that ω_0 is proportional to k. The linearly stable ARTI mode ($k = 1.57\ \mu m^{-1}$) in Fig. 5(c) is excited by the large value of V_p,[14] which induces the oscillation of $\hat{\omega}$ at early times ($\hat{W} < 2$). Nonetheless, in this case, $\hat{\omega}$ can still come close to matching the fitting curve later.

In the work of Zhang *et al.*,[14,38] it was pointed out that ω_0 has different values at the same bubble penetration depth h_b in the ARTI simulations with different values of V_p. In this study, we investigate the penetration depth ratio h_s/h_b of the mixing width W_{b-s} with different values of V_p, as shown in Fig. 6(a). Since the relation between ω_0 and W_{b-s} is identical (Fig. 5), different values of V_p can lead to different h_s/h_b of the mixing width W_{b-s} and further result in different ω_0 at the same h_b. In addition, the 2D vorticity structure is very similar at the same W_{b-s} in the ARTI simulations with different values of V_p, as shown in Fig. 6(b). This indicates that the vorticity has a global feature, i.e., it is correlated with the bubble growth as well as the spike growth. This global feature is related to the entire process of vorticity evolution, in which the vorticity is generated near the spike tip and convected toward the bubble vertex.[23]

We further study the dependence of the asymptotic vorticity strength on the ablation velocity V_a. Figure 7(a) shows the evolution of ω_0 in single-mode ARTI simulations for different values of V_a, where ω_0 reaches its peak value ω_{peak} in the deep nonlinear regime ($W_{b-s} \sim 5\lambda$). The dependence of ω_{peak} on V_a is then plotted in Fig. 7(b) and can be fitted by the curve

$$\frac{\omega_{peak}\, r_d}{k} = 9.0\frac{V_a^{2.0}}{0.5 + V_a^{2.0}}.$$

ω_{peak} increases with V_a and saturates as $V_a \to 3.5\ \mu m/ns$. This result indicates that the relation between ω_0 and V_a is more complicated

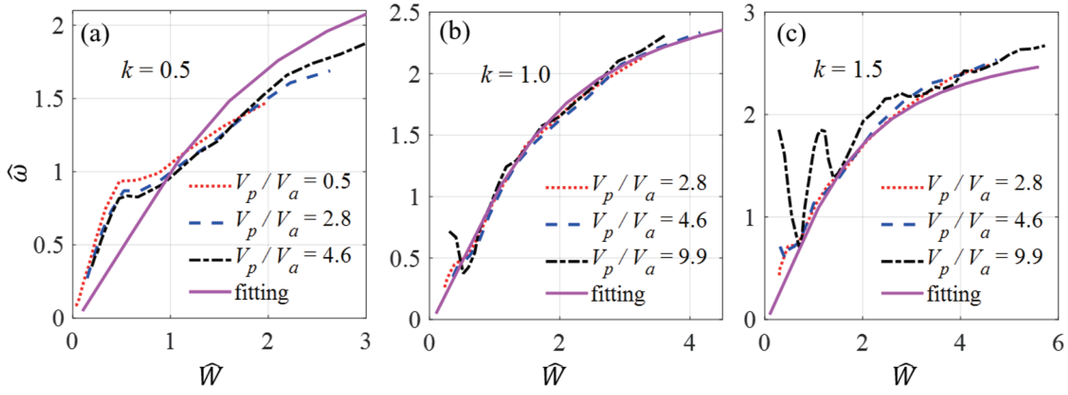

FIG. 5. (a)–(c) Evolution of the normalized vorticity strength $\hat{\omega}$ at the bubble vertex in single-mode ARTI simulations (V_a = 3.5 μm/ns) with different initial perturbation amplitudes V_p and wave numbers k (in μm^{-1}). $\hat{W} = W_{b-s}/\lambda$ is the normalized mixing width. The purple lines represent the same fitting curve.

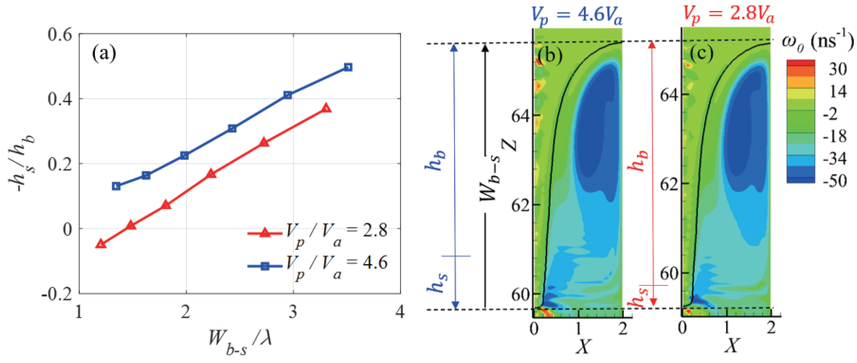

FIG. 6. (a) Evolution of the ratio of spike to bubble penetration depths, h_s/h_b, in single-mode ARTI simulations with different initial perturbation amplitudes V_p. (b) and (c) Comparison of 2D vorticity structures at the same mixing width W_{b-s} between single-mode ARTI simulations with $V_p = 4.6V_a$ (at 1.8 ns) and $2.8V_a$ (at 2.2 ns), respectively. The black line shows the ablation front interface.

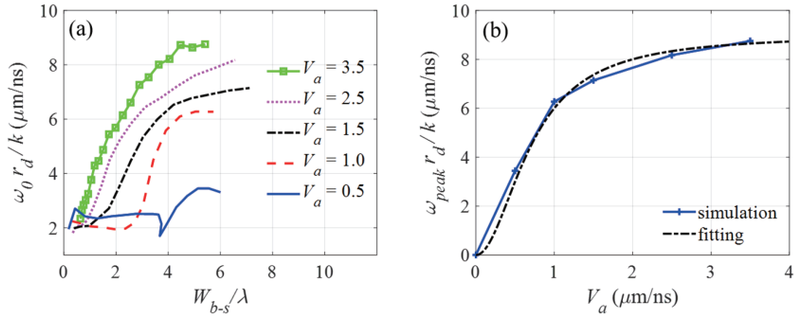

FIG. 7. (a) Evolution of the vorticity at the bubble vertex in single-mode ARTI simulations with different values of the ablation velocity V_a (in μm/ns). (b) Dependence of V_a on the peak value of the vorticity ω_{peak}. The black dot-dashed line is a fitting curve.

than the simple relation $\omega_0 \sim kV_a/r_d$ given in the work by Betti and Sanz.[23]

Finally, we conclude the relationship between the growth of the mixing width of single-mode ARTI and the evolution of the vorticity. The ARTI mixing width growth consists of bubble as well as spike growth. Even though the growth of the nonlinear spike is suppressed by the ablative effect (Sec. II), it can affect the ablation-generated vorticity, which in turn can affect the bubble acceleration. This vorticity is correlated with the mixing width W_{b-s}, for a given wave number k and ablation velocity V_a (Fig. 5). The initial perturbation amplitude can influence the vorticity strength (at the same h_b) by influencing the contributions of h_b and h_s to W_{b-s} (Fig. 6).

IV. ANALYTICAL MODEL FOR NONLINEAR GROWTH OF SINGLE-MODE ARTI

Since the evolution of the ablation-generated vorticity is related only to the growth of the mixing width, one can introduce the evolution of vorticity into the nonlinear growth of single-mode

ARTI. In this section, we present an analytical model developed for describing the nonlinear growth of single-mode ARTI [Eqs. (8) and (9)] by incorporating the effects of mass ablation (Sec. II) and the ablation-generated vorticity (Sec. III) into a CRTI model proposed by Mikaelian.[33,34]

In the linear growth regime, the penetration depths of the bubble and the spike $h_{b/s}$ in single-mode CRTI[1,2] can be written as

$$h_{b/s}^{CRT} = \pm h_0 \exp\left(\int_0^t \gamma_L^{cls} dt \right), \tag{3}$$

where h_0 is the initial perturbation amplitude. For ARTI, $h_{b/s}$ is defined as the distance from the bubble or spike vertex to the initial ablation front in the frame of an imploding shell. Thus, in the linear regime of single-mode ARTI, $h_{b/s}$ satisfies

$$h_{b/s}^{ART} = \pm h_0 \exp\left(\int_0^t \gamma_L^{abl} dt \right) + V_a t. \tag{4}$$

In Mikaelian's model,[33,34] the nonlinear growth of h_b in single-mode CRTI can be described by

$$h_b^{CRT} = h_{b0} + \frac{3 + A_T}{3(1 + A_T)k} \ln\left\{ \cosh\left[\frac{(6kA_T(1 + A_T)s)^{1/2}}{3 + A_T} \right] + \frac{\dot{h}_{b0}}{V_b^{cls}} \sinh\left[\frac{(6kA_T(1 + A_T)s)^{1/2}}{3 + A_T} \right] \right\}, \tag{5}$$

which is the solution of the potential flow model for an arbitrary A_T.[16] Here, $s = \left(\int_{t_{bNL}}^t \sqrt{g} dt \right)^2$, t_{bNL} is the transition time from the linear regime [Eq. (3)] to the nonlinear regime [Eq. (5)], and $h_{b0} = 1/3k$ and $\dot{h}_{b0}$ are the bubble amplitude and velocity, respectively, at the transition time. The CRTI spike can be expressed as[34]

$$-h_s^{CRT}(A_T) = h_b^{CRT}(A_T) \left\{ 1 + (0.4 + 0.6A_T^{10}) \left[\left(\frac{-h_s^{CRT}(1)}{h_b^{CRT}(A_T)} \right)^A - 1 \right] \right\}, \tag{6}$$

which is obtained by interpolation.

In the present study of CRTI, we use Eq. (5) to describe the nonlinear growth of h_b^{CRT}, the same as in Mikaelian's model. For the spike, an exponentially growing spike acceleration $\ddot{h}_s^{CRT}$ [Eq. (3)] is used, until it is equal to an effective acceleration $a_{eff}^{cls}(A_T, g)$, at which point $\ddot{h}_s^{CRT}$ is replaced by a_{eff}^{cls}. Thus, the nonlinear growth of h_s^{CRT} can be written as

$$h_s^{CRT} = \iint_{t_{sNL}}^t \ddot{h}_s dt^2 + \dot{h}_{s0}(t - t_{sNL}) + h_{s0}. \tag{7}$$

Here, t_{sNL} is the transition time from the linear regime [Eq. (3)] to the nonlinear regime [Eq. (7)], $\ddot{h}_s = -a_{eff}^{cls}$, and $\dot{h}_{s0}$ and h_{s0} are the spike velocity and amplitude, respectively, at the transition time t_{sNL}. The effective spike accelerations $a_{eff}^{cls}(A_T, g)$ are obtained by fitting the simulated CRTI results with Eq. (7). Four input parameters are required in this model: the gravitational acceleration g, the Atwood number A_T, the wave number k, and the initial perturbation amplitude h_0. Figure 8 compares the present spike model [Eq. (7)], Mikaelian's model [Eq. (6)], and the simulated h_s^{CRT}. It is found that the two models can describe the nonlinear growth of the CRTI spike when $0.5 \lesssim A_T \lesssim 0.9$.

Next, we consider the effect of ablation. The mass ablation and the associated vorticity effect are taken into account in the present model of single-mode CRTI [Eqs. (5) and (7)] for the description of the nonlinear growth of single-mode ARTI. In the nonlinear regime, the ARTI spike penetration depth h_s^{ART} has the same form as that of CRTI [Eq. (7)]

$$h_s^{ART} = h_s^{CRT} \quad \left(\ddot{h}_s = -a_{eff}^{abl} \right). \tag{8}$$

Here, a_{eff}^{abl} is obtained by fitting the simulated ARTI results with Eq. (8). The ablative effect on the nonlinear spike growth is represented by the difference between the effective spike accelerations in CRTI, a_{eff}^{cls}, and ARTI, a_{eff}^{abl}. Figure 9(a) shows the dependence of $a_{eff}^{cls,abl}$ on A_T in the conventional CRTI and the ARTI simulations. The fitting formula $a_{eff}/g = 0.777 A_T^{4.797} + a_{fit}$ is used here, where the fitting parameter a_{fit} [Fig. 9(b)] controls the shift of the fitting curve. It is found that the relation between a_{fit} and V_a can be fitted by $a_{fit} = -0.041 V_a + 0.130$. Owing to the ablative effect, the $A_T - a_{eff}/g$ curve of ARTI shifts downward compared with that of conventional CRTI. It is also found that the analytical expression of Sanz *et al.*[31] for asymptotic spike acceleration (data not shown in figure) can roughly describe a_{eff}^{abl} in the current model.

Similar to the nonlinear spike growth discussed in Sec. II, the nonlinear ARTI bubble evolution can also be divided into a potential flow regime and a reacceleration regime. When ARTI

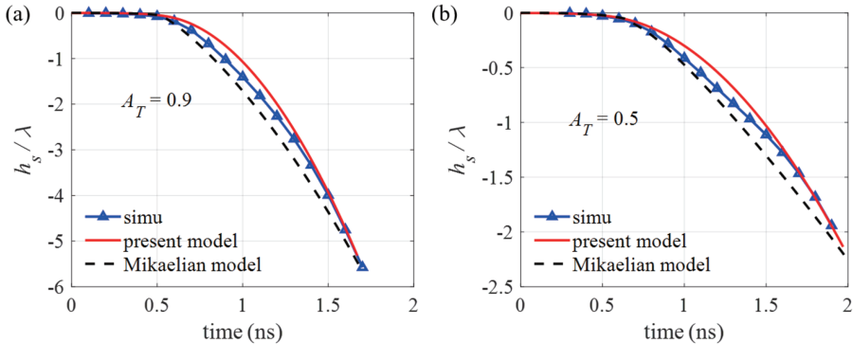

FIG. 8. Comparison of the evolution of the spike amplitude in conventional single-mode CRTI simulations, the present model, and Mikaelian's model at (a) $A_T = 0.9$ and (b) $A_T = 0.5$.

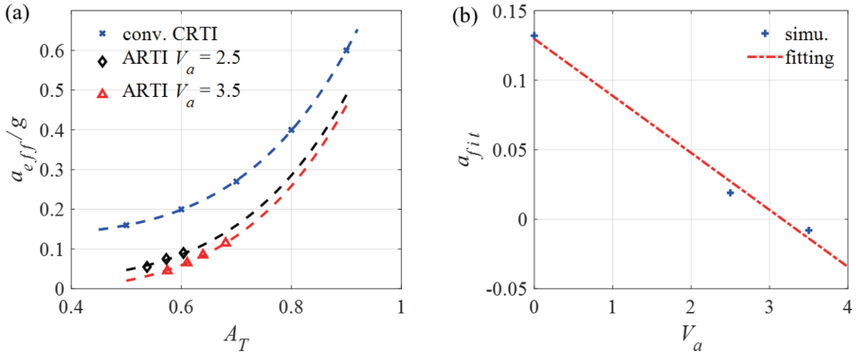

FIG. 9. (a) Dependence of effective spike acceleration a_{eff} on A_T in the conventional CRTI and the ARTI simulations. The dashed lines represent the fitting curves. (b) Dependence of the fitting coefficient a_{fit} on the ablation velocity V_a (in μm/ns). The red dot-dashed line is a linear fit.

is linearly stable ($k \gtrsim k_c$), a finite initial perturbation amplitude is required to destabilize the mode.[13,14] Therefore, ARTI growth can begin in the nonlinear regime with a strong vorticity effect.[14] When ARTI is linearly unstable ($k < k_c$), the bubble evolution in the potential flow regime tends to be classical, because the effects of mass ablation and vorticity on bubble growth are negligible.[23] Thus, the expression for the ARTI bubble penetration depth h_b^{ART} in the potential flow regime has the same form as the classical expression given by Eq. (5). At the transition time $t_{b\text{NL}}$ from the linear to the potential flow regime, the bubble penetration depth and velocity are given by $h_{b0} = h_b^{ART}(t_{b\text{NL}}) = 1/3k + V_a t_{b\text{NL}}$ and $\dot{h}_{b0} = \dot{h}_b^{ART}(t_{b\text{NL}})$, respectively.

In the reacceleration regime, the bubble is accelerated by the vorticity-induced centrifugal force F_c, which is opposite to the inertial acceleration g. Together with the bubble buoyancy force F_b, the total force per unit volume acting on the bubble element is increased from $F_b = \rho_h g - \rho_l g$ to

$$F_b + F_c \approx \rho_h g - \rho_l g + \frac{3\rho_l \omega_0^2}{4k} = \rho_h \left[(1 - r_d) g + \frac{3 r_d \omega_0^2}{4k} \right].$$

The quasi-constant bubble velocity can be rewritten as

$$V_b^{abl} \approx \sqrt{\frac{2A}{3(1+A)} \frac{g}{k} + \frac{r_d \omega_0^2}{4k^2}} \approx V_b^{cls} \sqrt{1 + \frac{F_c}{F_b}},$$

where the ratio F_c/F_b represents the importance of vorticity in accelerating the bubble. It is found that the expression for V_b^{abl} agrees well with the simulated results when $F_c/F_b > 0.3$ is chosen as the criterion for the transition from the potential flow regime [Eq. (5)] to the reacceleration regime. The bubble penetration depth can then be obtained by simple numerical integration:

$$h_b^{ART} = h_b^{ART}(t_{vort}) + \int_{t_{vort}}^{t} V_b^{abl}(W_{b-s})\, dt, \tag{9}$$

where t_{vort} is the time at which the criterion $F_c/F_b > 0.3$ is reached. It should be noted that V_b^{abl} is affected by ω_0, and further by W_{b-s}, as indicated in Sec. III. This implies that the nonlinear bubble growth is affected by the spike growth, owing to the vorticity, and to obtain h_b^{ART}, the expression for h_s^{ART} [Eq. (8)] should be known in advance.

In comparison with the CRTI model [Eqs. (3), (5), and (7)], the only additional input parameter in the ARTI model [Eqs. (4), (5), (8), and (9)] is V_a. For the acceleration $g(t)$ in the model, we obtain the time history of the inertial acceleration from the simulations, which depends on V_a and the target equilibria (i.e., density and pressure). In addition, the initial amplitude h_0 in the model is different from the initial velocity perturbation amplitude V_p in the simulations. It is found that the relation between h_0 and V_p can be described by the simple expression $h_0 \approx 0.085 V_p/\gamma_L^{abl}$ for ARTI, whereas the expression is $h_0 \approx 0.15 V_p/\gamma_L^{cls}$ for CRTI.

The results of the ARTI model and the simulations are compared in Fig. 10. The predictions of the model are in good agreement with the simulation results, within an error of 5% for the bubble

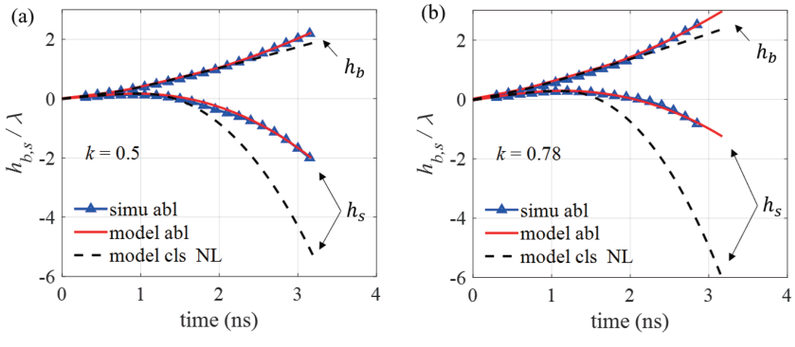

FIG. 10. Comparison of the evolution of the bubble and spike penetration depths h_b and h_s, respectively, from the single-mode ARTI simulations (with V_a = 3.5 μm/ns), the present ARTI model, and the present model using the classical forms [Eqs. (5) and (7)] in the nonlinear regime at (a) k = 0.5 μm^{-1} and (b) k = 0.78 μm^{-1}.

growth and 20% for the spike growth. When the effects of mass ablation and vorticity are excluded from the model [i.e., when Eqs. (5) and (7) are used], the growth in the mixing width ($W_{b-s} = h_b - h_s$) growth has a smaller contribution from h_b and a considerably larger contribution from h_s than the simulation results. It should be noted that these deviations increase with k because of the increasingly stronger effects of mass ablation and vorticity. For large k, the comparison indicates that the nonlinear W_{b-s} growth induced by the single mode is dominated by spike growth for CRTI, whereas it is dominated by bubble growth for ARTI.

The analytical ARTI model can describe the simulation results satisfactorily for the linearly unstable modes ($k < k_c$) with a small initial perturbation amplitude ($h_0 < 0.1\lambda$). However, when ARTI is linearly stable, a large initial perturbation amplitude is required to destabilize it. Hence, the ARTI growth starts directly from the nonlinear regime. In this case, it is found that the present model deviates from the simulation results.

V. CONCLUSION

In this work, the effect of ablation on the nonlinear spike growth of single-mode ARTI has been studied. The results of simulations show that the ablative effect can reduce the quasi-constant velocity and significantly suppress the reacceleration of the spike in the nonlinear phase owing to mass ablation and vorticity convection. It is also observed that the ARTI spike growth can affect the ablation-generated vorticity, which in turn can affect the bubble acceleration in the nonlinear phase. This vorticity is correlated with the mixing width for a given wave number and ablation velocity. The initial perturbation amplitude can influence the vorticity strength (at the same h_b) by influencing the contribution of h_b to the mixing width. Finally, an analytical model has been developed for the nonlinear growth of single-mode ARTI. The predictions of this model are in good agreement with the data from numerical simulations. It has been shown that the nonlinear growth of the mixing width induced by the single mode is dominated by bubble growth for small-scale (large-k) ARTI, whereas it is dominated by spike growth for CRTI.

ACKNOWLEDGMENTS

The authors would like to thank Y. S. Zhang, Z. Yan, and C. Meng for the useful discussions and technical support.

AUTHOR DECLARATIONS

Conflict of Interest

The authors have no conflicts to disclose.

Author Contributions

J. Y. Fu: Investigation (equal); Software (equal); Validation (equal); Visualization (equal); Writing – original draft (equal). **H. S. Zhang**: Funding acquisition (equal); Project administration (equal); Supervision (equal); Writing – review & editing (equal). **H. B. Cai**: Methodology (equal); Validation (equal); Writing – review & editing (equal). **P. L. Yao**: Methodology (equal); Validation (equal). **S. P. Zhu**: Methodology (equal); Validation (equal).

DATA AVAILABILITY

The data that support the findings of this study are available from the corresponding author upon reasonable request.

REFERENCES

[1]G. I. Taylor, "The instability of liquid surfaces when accelerated in a direction perpendicular to their planes. I," Proc. R. Soc. London, Ser. A **201**, 192 (1950).
[2]L. Rayleigh, *Scientific Papers* (Cambridge University Press, Cambridge, UK, 1900), Vol. II, p. 200.
[3]J. D. Lindl, *Inertial Confinement Fusion* (Springer-Verlag, New York, 1998), p. 11.
[4]V. N. Gamezo, A. M. Khokhlov, E. S. Oran, A. Y. Chtchelkanova, and R. O. Rosenberg, "Thermonuclear supernovae: Simulations of the deflagration stage and their implications," Science **299**, 77 (2003).
[5]R. S. Craxton, K. S. Anderson, T. R. Boehly, V. N. Goncharov, D. R. Harding *et al.*, "Direct-drive inertial confinement fusion: A review," Phys. Plasmas **22**, 110501 (2015).
[6]A. R. Bell, "Turbulent amplification of magnetic field and diffusive shock acceleration of cosmic rays," Mon. Not. R. Astron. Soc. **353**, 550 (2004).
[7]S. E. Bodner, "Rayleigh-Taylor instability and laser-pellet fusion," Phys. Rev. Lett. **33**, 761 (1974).
[8]H. Takabe, K. Mima, L. Montierth, and R. L. Morse, "Self-consistent growth rate of the Rayleigh–Taylor instability in an ablatively accelerating plasma," Phys. Fluids **28**, 3676 (1985).
[9]J. Sanz, "Self-consistent analytical model of the Rayleigh-Taylor instability in inertial confinement fusion," Phys. Rev. Lett. **73**, 2700 (1994).
[10]R. Betti, V. N. Goncharov, R. L. McCrory, and C. P. Verdon, "Self-consistent cutoff wave number of the ablative Rayleigh–Taylor instability," Phys. Plasmas **2**, 3844 (1995).
[11]V. N. Goncharov, R. Betti, R. L. McCrory, and C. P. Verdon, "Self-consistent stability analysis of ablation fronts with small Froude numbers," Phys. Plasmas **3**, 4665 (1996).
[12]R. Betti, V. N. Goncharov, R. L. McCrory, and C. P. Verdon, "Growth rates of the ablative Rayleigh–Taylor instability in inertial confinement fusion," Phys. Plasmas **5**, 1446 (1998).
[13]J. Sanz, R. Betti, R. Ramis, and J. Ramírez, "Nonlinear theory of the ablative Rayleigh–Taylor instability," Plasma Phys. Controlled Fusion **46**, B367 (2004).
[14]H. Zhang, R. Betti, V. Gopalaswamy, R. Yan, and H. Aluie, "Nonlinear excitation of the ablative Rayleigh-Taylor instability for all wave numbers," Phys. Rev. E **97**, 011203(R) (2018).
[15]D. Layzer, "On the instability of superposed fluids in a gravitational field," Astrophys. J. **122**, 1 (1955).
[16]V. N. Goncharov, "Analytical model of nonlinear, single-mode, classical Rayleigh-Taylor instability at arbitrary Atwood numbers," Phys. Rev. Lett. **88**, 134502 (2002).
[17]D. Oron, L. Arazi, D. Kartoon, A. Rikanati, U. Alon, and D. Shvarts, "Dimensionality dependence of the Rayleigh–Taylor and Richtmyer–Meshkov instability late-time scaling laws," Phys. Plasmas **8**, 2883 (2001).
[18]S. I. Sohn, "Vortex model and simulations for Rayleigh-Taylor and Richtmyer-Meshkov instabilities," Phys. Rev. E **69**, 036703 (2004).
[19]X. He, R. Zhang, S. Chen, and G. D. Doolen, "On the three-dimensional Rayleigh–Taylor instability," Phys. Fluids **11**, 1143 (1999).
[20]P. Ramaprabhu and G. Dimonte, "Single-mode dynamics of the Rayleigh-Taylor instability at any density ratio," Phys. Rev. E **71**, 036314 (2005).

[21] P. Ramaprabhu, G. Dimonte, P. Woodward, C. Fryer, G. Rockefeller *et al.*, "The late-time dynamics of the single-mode Rayleigh-Taylor instability," Phys. Fluids **24**, 074107 (2012).
[22] J. P. Wilkinson and J. W. Jacobs, "Experimental study of the single-mode three-dimensional Rayleigh-Taylor instability," Phys. Fluids **19**, 124102 (2007).
[23] R. Betti and J. Sanz, "Bubble acceleration in the ablative Rayleigh-Taylor instability," Phys. Rev. Lett. **97**, 205002 (2006).
[24] R. Yan, R. Betti, J. Sanz, H. Aluie, B. Liu, and A. Frank, "Three-dimensional single-mode nonlinear ablative Rayleigh-Taylor instability," Phys. Plasmas **23**, 022701 (2016).
[25] T. Wei and D. Livescu, "Late-time quadratic growth in single-mode Rayleigh-Taylor instability," Phys. Rev. E **86**, 046405 (2012).
[26] A. Hamzehloo, P. Bartholomew, and S. Laizet, "Direct numerical simulations of incompressible Rayleigh–Taylor instabilities at low and medium Atwood numbers," Phys. Fluids **33**, 054114 (2021).
[27] L. Duchemin, C. Josserand, and P. Clavin, "Asymptotic behavior of the Rayleigh-Taylor instability," Phys. Rev. Lett. **94**, 224501 (2005).
[28] J. O. Kane, H. F. Robey, B. A. Remington, R. P. Drake, J. Knauer *et al.*, "Interface imprinting by a rippled shock using an intense laser," Phys. Rev. E **63**, 055401(R) (2001).
[29] A. Casner, V. A. Smalyuk, L. Masse, I. Igumenshchev, S. Liberatore *et al.*, "Designs for highly nonlinear ablative Rayleigh-Taylor experiments on the National Ignition Facility," Phys. Plasmas **19**, 082708 (2012).
[30] L. F. Wang, W. H. Ye, X. T. He, W. Y. Zhang, Z. M. Sheng *et al.*, "Formation of jet-like spikes from the ablative Rayleigh-Taylor instability," Phys. Plasmas **19**, 100701 (2012).
[31] J. Sanz, J. Ramírez, R. Ramis, R. Betti, and R. P. J. Town, "Nonlinear theory of the ablative Rayleigh-Taylor instability," Phys. Rev. Lett. **89**, 195002 (2002).
[32] W. H. Ye, L. F. Wang, and X. T. He, "Spike deceleration and bubble acceleration in the ablative Rayleigh–Taylor instability," Phys. Plasmas **17**, 122704 (2010).
[33] K. O. Mikaelian, "Explicit expressions for the evolution of single-mode Rayleigh-Taylor and Richtmyer-Meshkov instabilities at arbitrary Atwood numbers," Phys. Rev. E **67**, 026319 (2003).
[34] K. O. Mikaelian, "Solution to Rayleigh-Taylor instabilities: Bubbles, spikes, and their scalings," Phys. Rev. E **89**, 053009 (2014).
[35] L. Spitzer and R. Härm, "Transport phenomena in a completely ionized gas," Phys. Rev. **89**, 977 (1953).
[36] J. Xin, R. Yan, Z.-H. Wan, D.-J. Sun, J. Zheng *et al.*, "Two mode coupling of the ablative Rayleigh-Taylor instabilities," Phys. Plasmas **26**, 032703 (2019).
[37] H. Zhang, R. Betti, R. Yan, D. Zhao, D. Shvarts, and H. Aluie, "Self-similar multimode bubble-front evolution of the ablative Rayleigh-Taylor instability in two and three dimensions," Phys. Rev. Lett. **121**, 185002 (2018).
[38] H. Zhang, R. Betti, R. Yan, and H. Aluie, "Nonlinear bubble competition of the multimode ablative Rayleigh–Taylor instability and applications to inertial confinement fusion," Phys. Plasmas **27**, 122701 (2020).
[39] P. W. McKenty, V. N. Goncharov, R. P. J. Town, S. Skupsky, R. Betti, and R. L. McCrory, "Analysis of a direct-drive ignition capsule designed for the National Ignition Facility," Phys. Plasmas **8**, 2315 (2001).
[40] X. Bian, H. Aluie, D. Zhao, H. Zhang, and D. Livescu, "Revisiting the late-time growth of single-mode Rayleigh–Taylor instability and the role of vorticity," Physica D **403**, 132250 (2020).
[41] L. F. Wang, C. Xue, W. H. Ye, and Y. J. Li, "Destabilizing effect of density gradient on the Kelvin–Helmholtz instability," Phys. Plasmas **16**, 112104 (2009).
[42] L. F. Wang, W. H. Ye, and Y. J. Li, "Numerical investigation on the ablative Kelvin-Helmholtz instability," Europhys. Lett. **87**, 54005 (2009).